NANO LETTERS

2006
Vol. 6, No. 5
995−999

Differential Ion Transport Induced Electroosmosis and Internal Recirculation in Heterogeneous Osmosis Membranes

R. Qiao,† J. G. Georgiadis, and N. R. Aluru*

Department of Mechanical and Industrial Engineering, Beckman Institute for Advanced Science & Technology, NSF Science & Technology Center of Advanced Materials for Purifcation of Water with Systems, University of Illinois at Urbana-Champaign, Urbana, Illinois 61801, and Department of Mechanical Engineering, Clemson University, Clemson, South Carolina 29631

Received February 2, 2006; Revised Manuscript Received March 23, 2006

ABSTRACT

Water and ion transport through a heterogeneous membrane separating two electrolyte solutions at different concentrations is investigated by using molecular dynamics simulations. The membrane features pairs of oppositely charged pores with identical diameters. Simulation results indicate that the differential transport of K^+ and Cl^- ions through the membrane pores creates an electrical potential difference across the membrane, which then induces an electroosmotic water flux. The induced electroosmosis creates an internal recirculation loop of water between adjacent pores. The implications of these new observations are discussed.

Water transport through artificial or natural membranes by osmosis is of fundamental importance in many engineering and biological applications, for example, water purification, fuel cells, hydration of biological cells,[1−3] and so forth. An atomic-level understanding of the osmosis-related phenomena is crucial to gaining fundamental insight into the functioning of biological systems and for improving the design of engineering systems. Molecular dynamics (MD) simulation is a useful tool to elucidate the physical mechanisms governing osmosis. Although earlier MD simulations focused primarily on the osmosis phenomena of Lennard-Jones (LJ) fluids through model membranes,[4] recent studies have been extended to the osmotic transport of water through engineered and biological membranes.[5−8] Although these studies have improved our understanding of osmosis, many important issues in osmotic transport in complex systems still remain unaddressed.[9,10] For example, in almost all studies, the membrane pores are considered to be totally impermeable to the solute molecules. Although real membranes contain pores of different size or charge characteristics, this heterogeneity is seldom addressed although it has been proposed as a viable hypothesis.[11] In this paper, we report on the MD simulation of osmotic transport of water through leaky membranes featuring pairs of oppositely charged pores. We show that, because of the differential transport of ions through the two pores, an electrical potential difference is set up across the membrane and this induces electroosmosis. The induced electroosmosis generates an internal recirculation loop of water, which can have important implications in engineering and biological applications. For example, internal circulation of water is observed in live plant roots[12] and the present study can elucidate some of the basic physical mechanisms governing water and ion transport in plant tissues.

Figure 1a and b shows the schematic and a rendered snapshot of the simulation system, respectively. The system consists of two square membranes (5.1 nm long along x and y directions and 1.5 nm thick) separating two KCl solutions of different concentrations. Two pores of identical diameter ($d_p = 1.4$ nm) are inserted through each membrane. The center of each pore is located along the diagonal of the square membrane with a center-to-center distance of 3.61 nm. Atoms on the pore surfaces are assigned small charges to produce a net charge density of ± 0.12 C/m^2. The dimensions of the solution chambers connecting each membrane are shown in Figure 1a. Periodic boundary conditions are used in all three directions.[4−7] Both the membrane and the pore atoms are frozen to their original lattice and are modeled as Lennard-Jones (LJ) atoms with parameters for that of carbon.[13] Water is modeled by using the SPC/E model, and ions are modeled as charged LJ atoms.[14]

* Corresponding author. E-mail: aluru@uiuc.edu.
† Clemson University.

10.1021/nl060253b CCC: $33.50
Published on Web 04/07/2006

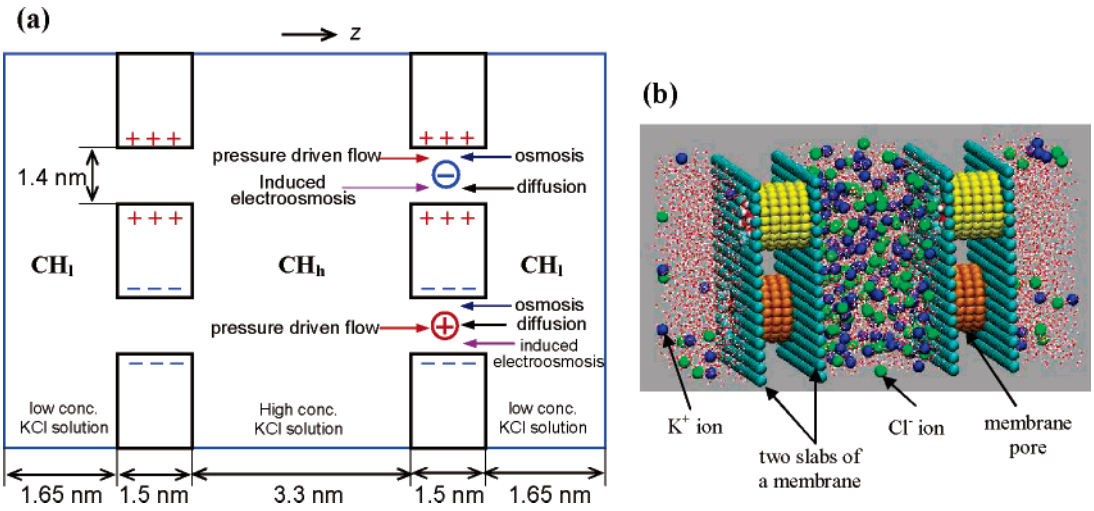

Figure 1. (a) Sketch of the simulation system. The various physical mechanisms, along with their directions, that could play a role in the transport of water are represented by arrows, and the water recirculation loop is also shown. The fluxes are symmetrical in the left membrane. CH_l denotes the low ion concentration chamber, and CH_h denotes the high ion concentration chamber. (b) A snapshot (rendered using VMD[23]) of the simulation system.

MD simulations were performed with a modified Gromacs 3.0.5[15] at constant volume and temperature. The temperature of the fluid was maintained at 300 K by using a Berendsen thermostat. A cutoff scheme was used to compute the LJ potential. The electrostatic interactions were computed by using the particle mesh Ewald method.[16] We started the simulation by filling the two chambers with KCl solutions of different concentration. A 500 ps simulation was first performed to allow the water molecules and ions to enter the membrane pores. Then, we generated five different initial configurations of the system by perturbing the position and velocity of the atoms in the original system. After that, the water molecules and ions in the pores were position-restrained and the system was simulated for another 500 ps for each of the initial configurations. Subsequently, the position restraints on the water and ions in the membrane pores were removed and a production run of 14 ns was performed for each of the five systems. At the beginning of the production run, the KCl concentration is about 0.40 and 2.32 M in the two chambers, respectively. At the beginning of the simulation, the pressure of the solution in the two chambers was approximately the same (~20 bar). The trajectory was saved every 2 ps during the production run, and the results reported below were obtained by averaging the simulation data generated from the production runs starting from the five different initial configurations. The flux across the membrane and the occupancy of water and ions in the two chambers were computed by tracking the water molecules and ions in the system, and the hydrostatic pressure of the electrolyte solution in the two chambers was computed by measuring the force acting on the membrane atoms.

Figure 2 shows the evolution of the water occupancy in the two chambers. We observe that during the first nanosecond, the water in the low ion concentration chamber (CH_l) migrates into the high ion concentration chamber (CH_h) quickly. After that, the water occupancy in the two chambers changes very slowly. This is due to the fact that at the beginning of the simulation the water transport is dominated by the osmosis of water from CH_l to CH_h. As the water occupancy in CH_h increases, the hydrostatic pressure in CH_h increases quickly while the pressure in CH_l drops at the same time. This then generates a pressure-driven flow of water from CH_h to CH_l (see Figure 1). At a later time, the water fluxes due to these two processes tend to cancel each other. This canceling effect, along with the electroosmotic flow of water across the leaky membrane (discussed next), leads to the slow variation of water occupancy in the two chambers. The canceling effect also indicates that the streaming current caused by the convective transport of the counterions is negligible. Figure 3 shows the variation of the hydrostatic pressure in the two chambers, and we observe that a pressure difference across the membrane builds up within the first nanosecond, but varies slowly after that. The average pressure difference between the two chambers during the time period 3.5−14 ns is found to be 64 ± 10.5 bar. Because the water occupancy varies very slowly between 3.5 and 14 ns, we can estimate the pressure difference by using the van't Hoff's

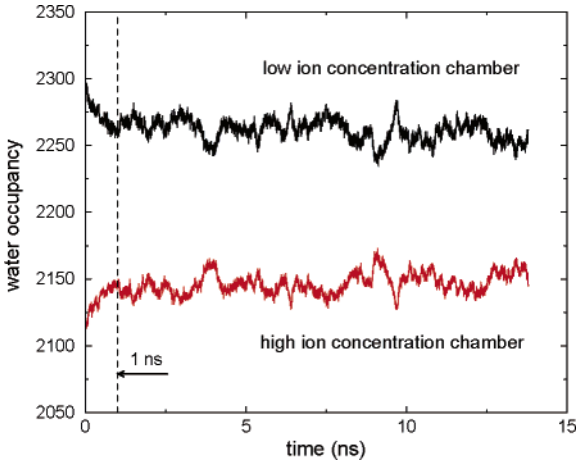

Figure 2. Evolution of the water occupancy in the two chambers with time.

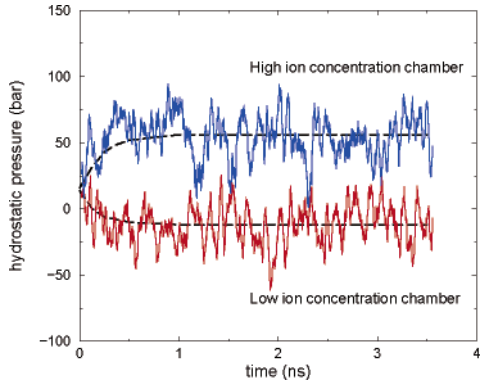

Figure 3. Evolution of the hydrostatic pressure in the two chambers during the first 3.5 ns of the simulation. The dashed lines are guides for the eyes.

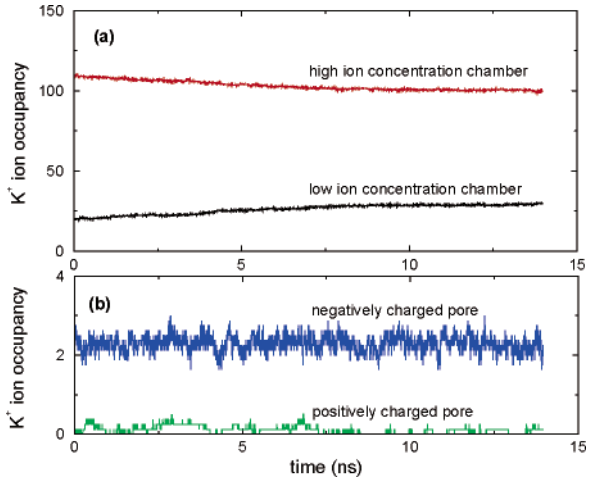

Figure 4. Evolution of the K^+ ion occupancy in the two solution chambers (a) and in the membrane pores (b) with time.

relation,[3] $\Delta P = \sigma RT\Delta\bar{C}$, where σ is the reflection coefficient ($\sigma = 1.0$ for ideal semipermeable membranes where ions cannot enter the membrane pores), R is the gas constant, T is the absolute temperature, and $\Delta\bar{C}$ is the average solute concentration difference between the two chambers. In our simulation, $\Delta\bar{C}$ is found to be 3.58 M, and this gives a ΔP of 89.1 bar if σ is taken as 1.0. Because this prediction is higher compared to the observed value (64 bar), this indicates that the reflection coefficient is smaller than 1.0 ($\sigma = 0.72$). This is consistent with the observation (discussed next) that the membrane is leaky.

Figure 4a and b shows the evolution of the K^+ ion occupancy in the two chambers and in the membrane pores. We observe that over a time period of 14 ns about 11 K^+ ions are transported from CH_h to CH_l (the variance for the five different runs is about 1.5), confirming that the membrane is leaky in our simulations. Figure 4b indicates that K^+ ions are effectively rejected from the positively charged pore (average occupancy per pore is 0.11) and the transport of K^+ ions occurs mainly through the negatively charged pores. Analysis of the Cl^- ion occupancy in the two pores indicates that the Cl^- ions are almost completely rejected from the negatively charged pores (average occupancy per pore is 0.04) and the Cl^- ion transport is mainly

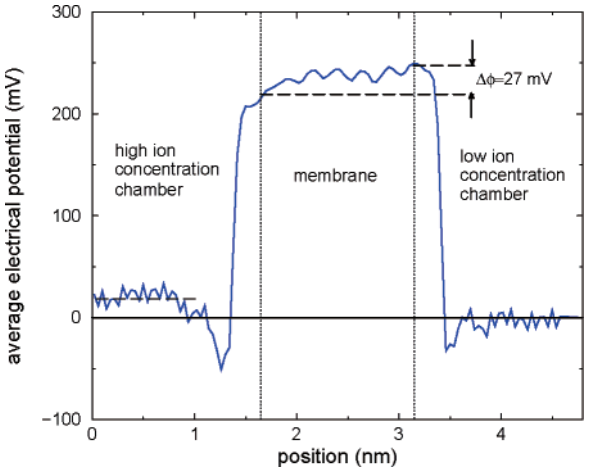

Figure 5. Time-averaged electrical potential ($\bar{\phi}(z)$) distribution in the simulation system during 2−4 ns. Because of the symmetry of the system with respect to the plane $z = 4.8$ nm, $\bar{\phi}(z)$ is shown only in half of the system. The dotted lines denote the surfaces of the membrane.

through the positively charged pores. The evolution of the Cl^- ion occupancy in the two chambers is essentially similar to that of the K^+ ion. However, separate equilibrium simulations indicated that the diffusion of the K^+ ion is 2.84 times faster compared to that of the Cl^- ion.[17] This observation is consistent with that reported in ref 18 and may be caused by the different hydrogen bonding of water inside the oppositely charged pores. Because of the faster diffusion of the K^+ ion compared to that of the Cl^- ion, the K^+ ions tend to accumulate faster in the low concentration chamber compared to the Cl^- ion, and this induces an electrical potential difference between the two chambers. This potential difference is usually referred to as the membrane diffusional potential[19]

$$\Delta\phi_{\text{diff}} = \frac{RT}{F}\frac{D_+ - D_-}{D_+ + D_-}\ln\frac{c_h}{c_l} \qquad (1)$$

where $\Delta\phi_{\text{diff}}$ and F are the membrane diffusional potential and the Faraday constant, respectively. D_+ and D_- are the diffusion coefficients of the positive and negative ions, respectively. c_h and c_l are the concentrations of the electrolyte solution separating the membrane. We computed $\Delta\phi_{\text{diff}}$ during the time period of 2.0−4.0 ns, when the average ion (K^+ or Cl^-) occupancy in the high and low concentration chambers is 106.2 and 22.5 (the variance for the five different runs is about 2.3), respectively. Using $D_+/D_- = 2.84$, eq 1 predicts a potential difference of 19.2 mV. Although the inhomogeneous nature of our system in the *xy* plane suggests that a three-dimensional analysis of the potential distribution is the most rigorous approach, such an analysis exceeds the present computational power. Instead, we compute the average potential $\bar{\phi}(z)$ in the z direction by using the method developed in refs 20 and 21. Figure 5 shows the time-averaged $\bar{\phi}(z)$ during $t = 2.0-4.0$ ns, and a potential drop of 27 ± 11 mV is observed across the membrane. Considering the ubiquitous statistical error in the MD results, the

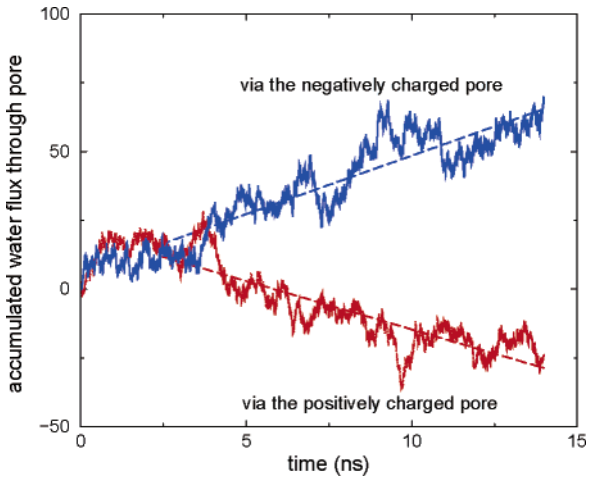

Figure 6. Accumulated water flux through the positive and negative membrane pores. The water flux $CH_l \rightarrow CH_h$ (i.e., the direction of osmosis) is defined as positive. The dashed lines are a linear fit to the accumulated flux from 2 to 14 ns.

quantitative agreement between the MD result and the prediction from eq 1 is reasonable.

The induced electrical potential difference across the membrane gives rise to a bilateral electroosmotic transport of water through the charged membrane pores. Ultimately, an electroosmotic flow in the direction of $CH_h \rightarrow CH_l$ through the positively charged pores and an electroosmotic flow in the direction of $CH_l \rightarrow CH_h$ through the negatively charge pores is expected (see Figure 1). Figure 6 shows the accumulated water flux in the positive and negative membrane pores. We observe that during the initial period of the simulation, that is, for $t < 2.0$ ns, the water flux in both pores is in the same direction ($CH_l \rightarrow CH_h$), indicating that osmosis dominates. However, after the initial 2.0 ns time period, the water transport is dominated by the electroosmotic flow because the osmosis is canceled substantially by the pressure-driven flow as discussed earlier. As a result, the direction of the water flux in the positive pore is reversed, and an internal water recirculation loop spanning the pore pair is observed. To estimate the strength of the internal recirculation, we fit the accumulated flux from $t = 2-14$ ns to a linear curve and find that the average transport rate of water, $\bar{q}$, through the positive and negative pores is 3.63 ± 1.28/ns (i.e., on an average about 3.63 water molecules go through the pore per nanosecond) and 4.22 ± 1.52/ns, respectively. Using the average water occupancy, $\bar{m}$, (38.3/pore for the positive pores and 37.6/pore for the negative pores), and the pore length ($L_p = 1.5$ nm), we estimate the mean transport velocity, $\bar{u} = 0.5\bar{q}L_p/\bar{m}$ to be 7.11×10^{-2} m/s and 8.42×10^{-2} m/s in the positive and negative pores, respectively. Because the magnitude of these two velocities is comparable, we will use the transport velocity in the positive pore for our discussion. To compare the strength of the convective transport with the diffusional transport, we define a membrane Peclet number, $Pe_m = UL_p/D$, where U is the convective velocity, L_p is the membrane thickness, and D is the diffusion coefficient. For a small solute molecule with a large diffusion coefficient, the Peclet number is small, indicating that its transport is dominated by diffusion. However, for the transport of solutes of larger molecular weight or larger particles with a smaller diffusion coefficient, the convective transport can become important. For example, for a bigger molecule with a diffusion coefficient of 1.0×10^{-12} m^2/s in the narrow nanopore,[22] Pe_m will be 107, indicating that the convective transport due to the induced electroosmosis can be much stronger compared to the diffusion. A relatively strong convective transport can have rich engineering and biological ramifications. For example, nanoparticles in the high ion concentration chamber shown in Figure 1 cannot normally enter the low ion concentration chamber because of their slow diffusion. However, when the convective transport is strong, these contaminants could pollute the low concentration chamber via this additional entrainment mechanism. Such heterogeneous membrane structures are ubiquitous in biological membranes. With the proviso that the system considered here is rather simplistic relative to the various ion gates that are embedded in the phospholipid bilayer of biological cells, our results point out to an additional transmembrane water flux mechanism. Although its biological analogue has not been observed directly, our model could inspire a class of active ion gate devices and permselective barriers employed in water management applications.

We note that the ion concentration in the two chambers is not maintained because our simulations were performed in the NVT ensemble. Owing to the leaky nature of the membrane pores, the concentration difference between the two chambers, and thus the diffusional potential, will gradually decay to zero, and the induced electroosmosis will disappear eventually. However, if the concentration difference does not diminish during the time period of observation (as in our simulation) or is maintained (as in most experiments), then the induced electroosmosis will be observed.

In summary, water and ion transport through a leaky membrane was studied by using MD simulations. Simulation results indicate that the differential transport of K^+ and Cl^- ions creates an electrical potential difference across the membrane, which then induces an electroosmotic flux of water and an internal recirculation of water in the system. The induced electroosmotic transport can influence the transport of nanoparticles or polymer chains with small diffusion coefficients substantially. Finally, in addition to the charge asymmetry of the membrane pores presented in this paper, there are many other possible mechanisms (e.g., ion selectivity achieved by varying the size of the nanopore, different cation and anion mobility, etc.) that can lead to the differential transport of ions, and thus an induced convective transport.

Acknowledgment. This research was supported by the NSF Sci. & Tech. Center of Advanced Materials for the Purification of Water with Systems (CAMPWS, cooperative agreement CTS-0120978) and a grant from NSF (0140496).

References

(1) van der Bruggen, B.; Vandecasteele, C.; Gestel, T. V.; Doyen, W.; Leysen, R. *Environ. Prog.* **2003**, *22*, 46−56.
(2) Friedman, M. H. *Principles and Models of Biological Transport*; Springer-Verlag: New York, 1986.

(3) Finkelstein, A. *Water Movement through Lipid Bilayers, Pores, and Plasma Membranes*; John Wiley & Sons: New York, 1987.
(4) Murad, S.; Powles, J. G. *J. Chem. Phys.* **1993**, *99*, 7271.
(5) Murad, S.; Oder, K.; Lin, J. *Mol. Phys.* **1998**, *95*, 401−408.
(6) Kotelyanskii, M. J.; Wagner, N. J.; Paulaitis, M. E. *J. Membr. Sci*. **1998**, *139*, 1−16.
(7) Kalra, A.; Garde, S.; Hummer, G. *Proc. Natl. Acad. Sci. USA* **2003**, *100*, 10175−10180.
(8) Zhu, F.; Tajkhorshid, E.; Schulten, K. *Biophys. J*. **2004**, *86*, 50.
(9) Tasaka, M.; Wada, C.; Nagasawa, M. *J. Membr. Sci*. **1980**, *6*, 171−183.
(10) Cervera, J.; Garcia-Morales, V.; Pellicer, J. *J. Phys. Chem. B.* **2003**, *107*, 8300−8309.
(11) Henzler, T.; Steudle, E. *J. Exp. Bot.* **1995**, *46*, 199−209.
(12) Steudle, E.; Peterson, C. A. *J. Exp. Biol*. **1998**, *49*, 775−788.
(13) Werder, T.; Walther, J. H.; Jaffe, R. L.; Halicioglu, T.; Koumoutsakos, P. *J. Phys. Chem. B.* **2003**, *107*, 1345−1352.
(14) Koneshan, S.; Rasaiah, J. C.; Lynden-Bell, R. M.; Lee, S. H. *J. Phys. Chem. B* **1998**, *102*, 4193−4204.
(15) Lindahl, E.; Hess, B.; van der Spoel, D. *J. Mol. Mod*. **2001**, *7*, 306−317.
(16) Darden, T.; York, D.; Pedersen, L. *J. Chem. Phys*. **1993**, *98*, 10089−10092.
(17) Separate md simulation was performed to study the diffusion of K^+ and Cl^- ions across the membrane. Specifically, both chambers were filled with 108 K^+ and Cl^- ions and 2118 water molecules, and a 9 ns equilibrium simulation was performed. During the simulation, the exchange of ions between the two chambers was monitored. We found that the exchange rate of K^+ and Cl^- ions in the two chambers was 2.12/ns and 0.75/ns, respectively. Because the exchange process is controlled by diffusion, we estimate the effective diffusion coefficient of the K^+ ion to be 2.84 times larger than that of the Cl^- ion.
(18) Qiao, R.; Aluru, N. R. *Colloids Surf., A* **2005**, *267*, 103−109.
(19) Heinz, E. *Electrical Potentials in Biological Membrane Transport*; Springer-Verlag: New York, 1981.
(20) Spohr, E. *J. Chem. Phys.* **1997**, *107*, 6342−6348.
(21) Sachs, J. N.; Crozier, P. S.; Woolf, T. B. *J. Chem. Phys.* **2004**, *121*, 10847−10851.
(22) Meller, A.; Nivon, L.; Branton, D. *Phys. Rev. Lett.* **2001**, *86*, 3435−3438.
(23) Humphrey, W.; Dalker, A.; Schulten, K. *J. Mol. Graphics* **1996**, *14*, 33−38.

NL060253B